Research Article | Vol. 28, No. 14 / 6 July 2020 / Optics Express 20503
Optics EXPRESS

High-performance stationary solar tracking through multi-objective optimization of beam-steering lens arrays

HÅKON J. D. JOHNSEN,[1,*] ASTRID AKSNES,[2] AND JAN TORGERSEN[1]

[1]Norwegian University of Science and Technology, Department of Mechanical and Industrial Engineering, Richard Birkelands Vei 2b, Trondheim, Norway
[2]Norwegian University of Science and Technology, Department of Electronic Systems, O.S. Bragstads plass 2b, Trondheim, Norway
[*]hakon.j.d.johnsen@ntnu.no

Abstract: Beam-steering lens arrays enable solar tracking using millimeter-scale relative translation between a set of lens arrays. This may represent a promising alternative to the mechanical bulk of conventional solar trackers, but until now a thorough exploration of possible configurations has not been carried out. We present an approach for designing beam-steering lens arrays based on multi-objective optimization, quantifying the trade-off between beam divergence and optical efficiency. Using this approach, we screen and optimize a large number of beam-steering lens array configurations, and identify new and promising configurations. We present a design capable of redirecting sunlight into a $<2^{\circ}$ divergence half-angle, with 73.4% average yearly efficiency, as well as a simplified design achieving 75.4% efficiency with a $<3.5^{\circ}$ divergence half-angle. These designs indicate the potential of beam-steering lens arrays for enabling low-cost solar tracking for stationary solar concentrators.

1. Introduction

Solar concentrators can provide highly concentrated solar power for applications such as concentrator photovoltaics (CPV), concentrated solar power (CSP), or solar lighting [1]. The concentrators require accurate solar tracking to achieve high concentration [2], which is usually performed by rotating the concentrator to face the sun. Recent work has considered the use of tracking-integrated systems that can track the sun without being rotated by an external solar tracker [3–7].

One approach is the concept of beam-steering, where a tracking-integrated system emits collimated light, which can be concentrated in a separate concentrator [3], as illustrated in Fig. 1(a). This approach allows the design of the concentrator optics to be independent of the design of the tracking optics, and it enables the beam-steering system to be used for different applications. Several beam-steering concepts have been proposed for solar tracking, including electrowetting to change the angle of the interface between two liquids with different refractive indices [8], microfluidic beam-steering arrays [9], rotating prism arrays [10], liquid crystals controlled by electric fields [11], rotating off-axis Fresnel lenses [12], and beam-steering lens arrays [13–15].

A beam-steering lens array consists of a set of lens arrays arranged in an afocal configuration, enabling beam-steering by relative lateral translation between the lens arrays [14], as illustrated in Fig. 1(b). The concept was originally proposed for steering of laser beams [16–18]. In 2012, Lin et al. proposed utilizing the same concept for single-axis solar tracking, while also proposing a design method based on the Simultaneous Multiple Surface (SMS) Method [13]. Johnsen

#396477 https://doi.org/10.1364/OE.396477
Journal © 2020 Received 1 May 2020; revised 18 Jun 2020; accepted 18 Jun 2020; published 25 Jun 2020

Optics EXPRESS

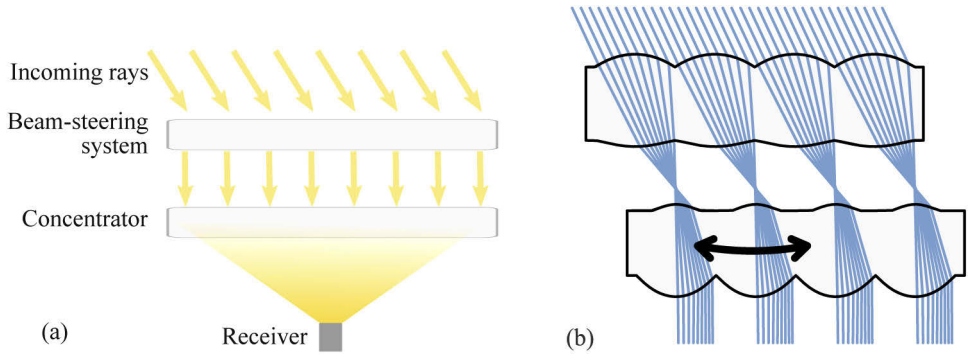

Fig. 1. (a) Conceptual illustration of how a beam-steering system can be combined with conventional concentrator optics. (b) Example of a beam-steering lens array: An afocal stack of lens arrays, which redirects sunlight utilizing relative movement between these lens arrays.

et al. extended the concept to two-axis solar tracking and demonstrated the use of numerical optimization for designing the systems [14,15].

By relying entirely on geometrical optics, beam-steering lens arrays have the benefit that they do not depend on special materials. This can make them compatible with conventional high-volume manufacturing methods such as injection molding or roll-to-roll processing. A successful design may, therefore, have a short path towards commercial implementation. However, the design of a beam-steering lens array requires a careful balancing of the different requirements of the system, such as tracking range, divergence of the outgoing sunlight, and optical efficiency.

In this paper, we numerically investigate the achievable performance of a large number of different beam-steering lens array configurations designed for stationary solar tracking applications. In order to optimize the systems, we propose and use a design method for beam-steering lens arrays based on multi-objective optimization. Section 2 contains a description of the concepts and requirements of beam-steering lens arrays. Section 3 introduces the optimization method and the optimization parameters selected in this work, including a classification scheme used to generate the different optimized configurations. In Section 4, we present the results of the numerical optimization, which are further discussed in Section 5.

2. Beam-steering lens arrays

Figure 2 shows the basic paraxial working principle of a basic beam-steering lens array with a pair of lens arrays stacked in an afocal configuration. The lens arrays are separated by their combined focal lengths $f_1 + f_2$. The system can track incoming sunlight at an angle ϕ by translating the last lens array a distance Δx such that it is always aligned with the image of the sun from the first lens array:

$$\Delta x = f_1 \tan \phi. \tag{1}$$

In order for all rays to reach the correct lenslet in the array L_2, the second focal length must be smaller than the first. This leads to an angular magnification factor M:

$$M = \frac{f_1}{f_2} = 1 + 2\frac{f_1}{d} \tan \phi_{max}, \tag{2}$$

where ϕ_{max} is the highest supported angle of incidence for the beam-steering lens array.

Sunlight has an inherent divergence half-angle of approximately $\theta = 0.27°$ [19], which is magnified by this angular magnification factor M after passing through a beam-steering lens array.

Optics EXPRESS

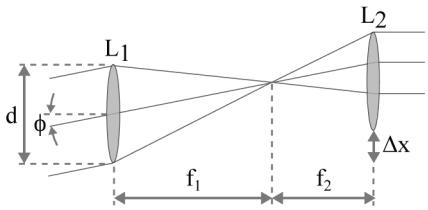

Fig. 2. Paraxial working principle of a simple beam-steering lens array.

The resulting divergence half-angle limits the maximum achievable concentration of a system with the configuration from Fig. 1(a) according to the fundamental limit to solar concentration for 2-axis concentration in air [2]:

$$C_{max} = \frac{1}{(\sin\theta)^2} \tag{3}$$

To allow high concentration ratios, it is therefore desirable that the angular magnification of the system is low. This leads to a trade-off between the tracking range ϕ_{max}, and divergence angle θ for this simple paraxial model of a beam-steering lens array.

It has been shown that this magnification factor can be eliminated in laser beam-steering systems by introducing an additional paraxial field lens to the system, where all three lens arrays have the same focal length f [17]. This shows the importance of design choices such as the number and order of surfaces when designing a beam-steering lens array. We call this the configuration of the system, which is a topic of investigation in this work.

While utilizing the same underlying principle, there are significant differences between earlier systems for steering of laser beams [16–18] and a system designed for solar tracking:

- In solar tracking, the beam-steering system receives sunlight from varying directions and emits it in a fixed direction. The earlier proposed laser systems [16–18] work in reverse, receiving the beam from a fixed direction and emitting in a variable direction.
- In laser systems, the lens arrays usually work in the diffractive regime, and additional phase-shifting optics are required to enable continuous beam-steering [17]. For solar tracking covering larger areas, the individual lenslets can be made large enough that the geometrical optical approximation is appropriate, and the separate lenslets can be considered individually.
- The steering range used in previously proposed laser systems is 5° to 15° [18,20,21], allowing design considerations based mainly on the paraxial approximation presented in this section. For stationary solar tracking, much larger steering angles are required, and the simple paraxial approximation presented in this section is no longer sufficient.
- In solar tracking, the system must be able to handle broadband sunlight, requiring chromatic aberration to be taken into account.

Based on these differences, we believe that a design method based on numerical optimization will be best able to handle the complexities and requirements of solar tracking applications.

3. Design method

We have utilized a numerical design method based on ray-tracing and numerical multi-objective optimization to design the beam-steering lens array systems. Numerical optimization is routinely used to design optical systems, and several studies of imaging optical systems have shown how the design space can be further explored by the use of multi-objective optimization algorithms,

Optics EXPRESS

identifying the trade-off between a set of competing system objectives [22–24]. In this section, we describe our design method, demonstrating how multi-objective optimization can also be utilized to design nonimaging optical system, and we specify the conditions for the results reported later in the paper.

3.1. Formulation of the optimization problem

We consider three main performance objectives for evaluating the performance of a complete beam-steering lens array:

- Maximizing the efficiency in redirecting sunlight.
- Minimizing the divergence of outgoing sunlight
- Minimizing the cost/complexity of the resulting system

The design of a beam-steering lens array can be considered a multi-objective optimization problem. An optimized solution must provide a reasonable trade-off between these objectives. Multi-objective optimization problems can be solved by finding a set of Pareto optimal solutions: solutions where the performance in one objective cannot be improved without degrading performance in another objective. In this way, the trade-off between objectives is quantified, allowing a designer to make an informed choice among the set of solutions [25].

Efficiency and divergence can be quantified as continuous objective functions, allowing a multi-objective optimization algorithm to map out the Pareto front between these objectives. Cost/complexity, on the other hand, is difficult to quantify and depends on several factors. Rather than quantify complexity directly, we consider cost/complexity to be influenced by the *configuration* of the beam-steering lens array – the sequence of surfaces and type of relative movements between them. We have chosen to optimize a broad set of configurations, enabling the comparison of different configurations with varying complexity, and allowing the selection of a configuration with the appropriate level of complexity for a specific use case. Cost/complexity can also be influenced by a number of other factors, including material selection, manufacturing tolerances, and optimization constraints for manufacturability - all of which are kept constant in the present work and may be considered more thoroughly in future work.

We formulated the following optimization problem:

$$\min \mathbf{f}\left(\mathbf{x}, \theta_{max}\right) = \left(-\overline{\eta}\left(\mathbf{x}, \theta_{max}\right), \theta_{max}\right) \tag{4}$$

$$\text{such that } g_j\left(\mathbf{x}\right) \leq 0, \tag{5}$$

where θ_{max} is the allowed divergence of outgoing sunlight, $\mathbf{x}$ is a set of free variables specifying the optical system (as listed in Table 2). $\overline{\eta}\left(\mathbf{x}, \theta_{max}\right)$ is the average yearly optical efficiency of the optical system subject to θ_{max}, as described in Section 3.2. The two components of $\mathbf{f}$ represent the two objectives: Maximizing the average yearly efficiency (minimizing $-\overline{\eta}$), while also minimizing the allowed divergence (minimizing θ_{max}). $g_j\left(\mathbf{x}\right)$ is a set of inequality constraints as listed in Table 3, ensuring manufacturability.

3.2. Average yearly efficiency

The metric of average yearly efficiency is inspired by the work from Ito et al., who elegantly showed that such a metric could be used to design a tracking-integrated system [26]. We define the average yearly optical efficiency as the fraction of yearly direct irradiation successfully redirected in the desired direction:

$$\overline{\eta}\left(\mathbf{x}, \theta_{max}\right) = \frac{E_{out}\left(\mathbf{x}, \theta_{max}\right)}{E_{in}}, \tag{6}$$

where E_{in} is the yearly direct irradiation received by the beam-steering lens array surface, and $E_{out}\left(\mathbf{x}, \theta_{max}\right)$ is the yearly irradiation successfully redirected within the permitted exit cone $\pm\theta_{max}$.

Optics EXPRESS

This average efficiency can be estimated by integrating across all angles of incidence ϕ:

$$\bar{\eta}\,(\mathbf{x}, \theta_{max}) = \int_0^{\pi} e\,(\phi) \times \eta\,(\mathbf{x}, \theta_{max}, \phi)\, d\phi, \tag{7}$$

where $e\,(\phi) = \frac{E_{in,\phi}(\phi)}{E_{in}}$ is the normalized angular distribution of irradiation received by the beam-steering lens array in its installed location. $\eta\,(\mathbf{x}, \theta_{max}, \phi)$ is the optical efficiency of the beam-steering lens for an optical system $\mathbf{x}$, a maximum divergence of outgoing sunlight θ_{max} and an angle of incidence ϕ.

In this work, we consider the beam-steering lens arrays to have a fixed orientation, tilted towards the equator with an angle equal to the latitude of the installation location, as illustrated in Fig. 3(a). As noted by Ito et al., this orientation gives a peak in irradiation distribution at $22° - 25°$ angle of incidence, irrespective of installation location [26]. We consider the beam-steering lens arrays optimized in this paper to be installed at a latitude of 40°. The location of 40° was chosen as an example to demonstrate the principle. However, as demonstrated by Schuster [27], this angular distribution is virtually independent of installation latitude when the panel is tilted according to installation latitude. We simulate the angular distribution of solar irradiation using Meinel and Meinel's air mass attenuation model [28] and for simplicity assume that cloud cover is not correlated to time of day or time of year. The resulting normalized irradiation distribution is shown in Fig. 3(b).

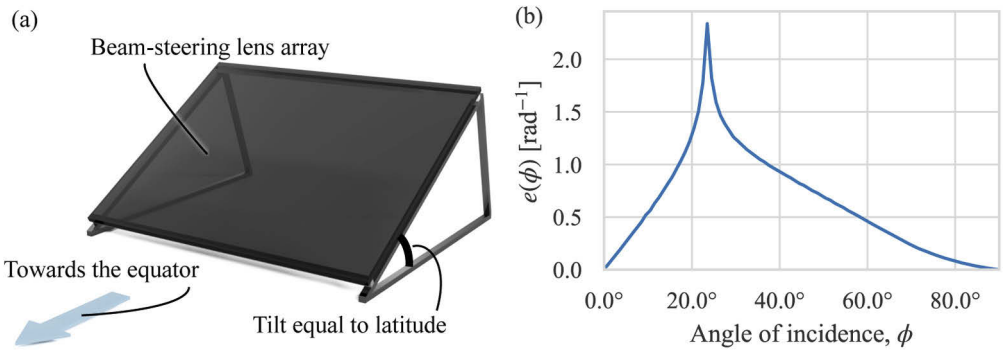

Fig. 3. (a) Assumed orientation of beam-steering lens array during optimization. (b) Simulated angular distribution of normalized yearly direct irradiation on a lens array with the fixed orientation from a, installed at a latitude of 40°.

With this formulation, the location of the installation location, weather data, and orientation of the beam-steering lens array are all contained in the normalized angular distribution of irradiation, $e\,(\phi)$, as shown in Eq. (7). The same formulation can therefore be used for optimizing beam-steering lens arrays with the details of a planned installation, by using the appropriate distribution $e\,(\phi)$. This may include real-world weather data, as well as other orientations, for instance being oriented east or west, or being mounted on single-axis external trackers.

It is worth noting that $\bar{\eta}$ in Eq. (6) is defined relative to the irradiation reaching the front surface of the beam-steering lens array while it is mounted in its chosen orientation. The cosine projection loss is therefore not included in the average efficiency, and will give an additional reduction in intensity compared to a system pointed directly towards the sun. On the other hand, fixed-orientation systems can increase power conversion per land area due to reduced shading between modules, as discussed by Price et al. [29]. These effects must be taken into account when comparing tracking-integrated systems to externally tracked systems, but have been considered to be beyond the scope of this work. Here, the aim is to compare different stationary systems that all share the same cosine projection loss.

Optics EXPRESS

3.3. Classifying different configurations

Previously proposed beam-steering lens array designs have utilized both single-sided [13] and double-sided [14] lens arrays, with relative lateral [30] or curved [13] tracking motion, and with both two [13], and three [31] lens arrays stacked together. In order to readily specify, compare, and evaluate different classes of designs, it can be useful to designate specific symbols for each of the components in a beam-steering lens array. Specific configurations of beam-steering lens arrays can then be described using a sequence of these symbols.

In this work, we use the set of symbols shown in Table 1.

The symbols from Table 1 can be used to classify both existing and new beam-steering lens array configurations. For instance:

- The example beam-steering lens array in Fig. 1: ◆⤸◆
- Lin et al., 2012 [13]: ◀⤸▶
- Watson, 1993 [17] (for steering of laser beams): ◆↓◆ and ◆↓◆▤◆
- Johnsen et al., 2018 [14]: ◆⤸◆ and ◀⤸◆⤸◆

Table 1. Proposed symbols for classifying different beam-steering lens array configurations.

Symbol[a]	Meaning
◀	Single-sided lens array with the flat side on the right.
▶	Single-sided lens array with the flat side on the left.
◆	Double-sided lens array
◀▶	A pair of single-sided lens arrays placed back-to-back, with index-matched lubricating oil between them supporting relative lateral translation between the lens arrays.
↓	Air-gap between lens arrays supporting a flat, lateral tracking trajectory.
⤸	Air-gap between lens arrays supporting a curved tracking trajectory.
▤	Air-gap between two surfaces, but no relative movement between the surfaces.

[a]The symbols are represented by the following Unicode [32] code-points: ◀=U+25C0, ▶=U+25B6, ◆=U+25C6, ↓=U+2193, ⤸=U+2938, ◀▶=U+25C0 U+200A U+25B6, ▤=U+25A4

3.4. Selecting configurations

Using the presented code for classifying beam-steering lens arrays, we have performed a comprehensive optimization of all possible combinations of the symbols in Table 1 with a maximum of 1 air-gap. This leads to a total of 52 configurations, of which 40 contains at least 1 movable surface. These configurations cover the range from complex configurations such as ◀▶⤸◀▶, to simple configurations such as ◀▶. Optimizing across this span can therefore give good insight into the trade-off between minimizing complexity and maximizing system performance.

3.5. Numerical optimization

The multi-objective optimization problem in Eq. (4) was solved using a memetic version of the MOEA/D-DE [33] multi-objective optimization algorithm. This algorithm decomposes the multi-objective problem into a set of scalarized sub-problems that are solved cooperatively.

Optics EXPRESS

We created the scalarized sub-problems by setting θ_{max} in Eq. (4) to fixed values in the range $0.5° \leq \theta_{max} \leq 5°$, which we assume to encompass the region of interest between high-accuracy and low-accuracy tracking. The MOEA/D implementation from Pymoo [34] was extended with the differential evolution strategy and the diversity preservation scheme proposed in the MOEA/D-DE algorithm [33]. The algorithm was then further extended to augment the global differential evolution with local searches based on SciPy's [35] implementation of the SLSQP optimization algorithm [36], as shown in Fig. 4. The resulting memetic optimization algorithm was run until convergence, with a limit of 10 000 iterations for each beam-steering lens array configuration.

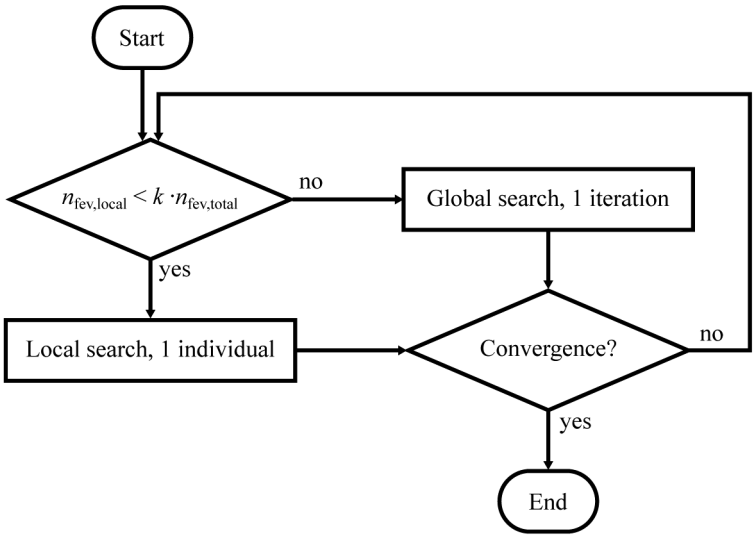

Fig. 4. The global MOEA/D-DE optimization algorithm is combined with the SLSQP local optimization algorithm to form a hybrid optimization algorithm. The choice between local and global search is based on the number of objective function evaluations in the local search, $n_{fev,local}$ compared to the total number of objective function evaluations, $n_{fev,total}$. We used $k = 0.5$, which means that 50% of the search effort is dedicated to the local searches.

The optimization workflow was managed using Snakemake [37]. Ray-tracing was performed using a custom sequential three-dimensional ray-tracer, as reported in previous work [14]. Hexagonal lens apertures were used for all simulations to simulate close packing in a lens array. Optimizations were performed across the AM1.5D solar spectrum [38], and all lenses were assumed to be made from Poly(methyl methacrylate) (PMMA). Reflection losses and chromatic aberration were taken into account, while absorption losses were not considered. The beam-steering lens array is a scale-invariant afocal system (as long as it is operated far away from the diffraction limit). Absorption losses depend on the dimensions of the system, which were not specified in these simulations. Reflection losses were estimated according to Fresnel's equations, taking the average of R_p and R_s and assuming that the light stays approximately unpolarized throughout the system. The angular distribution of sunlight was modeled using Buie's sunshape distribution model [39], assuming a circumsolar radiation of 5%. Average efficiency, according to Eq. (7), was estimated using multi-dimensional numerical integration with a quasi-Monte Carlo method implemented using a low-discrepancy Sobol sequence. Lens surfaces were represented as 8th order Forbes' Q^{con} surfaces [40], and the full set of free variables that was optimized is listed in Table 2. The lens arrays were optimized for as-built performance by assuming uniformly distributed positioning errors of $\pm 0.0025 \cdot T$ where T is the total thickness of the system, and assuming uniformly distributed slope errors in the surfaces of ±8 mrad, as listed in Table 3. If the

Optics EXPRESS

beam-steering lens array design is scaled to have a thickness of 20mm, this would correspond to a positioning error of 50 μm. In the ray-optical regime, errors such as curvature error, thickness error, surface waviness, or tracking error, all have the effect of changing the position and slope at the point where a ray intercepts a surface [2]. All these errors are therefore combined into the chosen error distribution for slope and position error. These errors were integrated into the quasi-Monte Carlo integration of Eq. (7) by sampling from these error distributions each time a ray crosses a surface, and this approach is further discussed in Section 5.2.

Table 2. List of free variables during optimization of the beam-steering lens arrays

Every surface	
R	Radius of curvature
k	Conic constant
a_1, a_2, a_3	Aspherical Q^{con} coefficients
t	Thickness
For the whole system	
c_1, c_2, c_3, c_4	Polynomial coefficients representing tracking motion
Every tracking motion (every ◄►, ↓, and ⤵)	
d	Proportionality constant for tracking motion
Every curved tracking motion (every ⤵)	
R_t	Radius of curvature of tracking geometry
k_t	Conic constant for tracking geometry
$a_{t,1}, a_{t,2}$	Q^{con} polynomial representing tracking geometry

In addition to assuming a fixed distribution of positioning and slope errors, the effect of these errors was further investigated by optimizing the ◄►↓◄► configuration for a set of different error distributions.

In each design, the lateral movements of the different lens arrays were constrained to be proportional to each other, allowing linked control, sharing the same mechanical actuator. The aspect ratio of each lens surface was constrained to be 0.5 or less, to prevent excessively curved lenses. Each lens array was constrained not to be thinner than half the lenslet diameter, to prevent too thin lens arrays, and also to be no thicker than 3 times the lenslet diameter, as summarized in Table 3.

These assumptions and constraints were chosen as an example of fairly permissive constraints, to explore a broad design space and get an overview of the performance of different configurations of beam-steering lens arrays. When planning a physical realization of such a system, these constraints would be modified according to the requirements of the chosen fabrication process.

Optics EXPRESS

Table 3. Manufacturing errors and manufacturing constraints assumed during optimization.

Assumed manufacturing errors (uniform distributions, T is total system thickness)	
Position error	$\pm 0.0025 \cdot T$
Slope error	±8mrad
Constraints (D is lenslet diameter)	
Lens thickness (thinnest point)	$>0.5 \cdot D$
Lens thickness (thickest point)	$<3 \cdot D$
Air gap thickness (thinnest point)	>0
Air gap thickness (thickest point)	$<2 \cdot D$
Lens aspect ratio	<0.5

4. Optimization results

The result of the numerical optimization is shown in Fig. 5. Each line represents a specific beam-steering lens array configuration, and each point along the line represents a specific design optimized for the particular trade-off between efficiency and divergence half-angle. Given the non-convex nature of the optimization problem, the optimization algorithm is not guaranteed to find the global optimum. The resulting Pareto front therefore only gives a lower bound on achievable efficiency for a specific configuration and divergence half-angle.

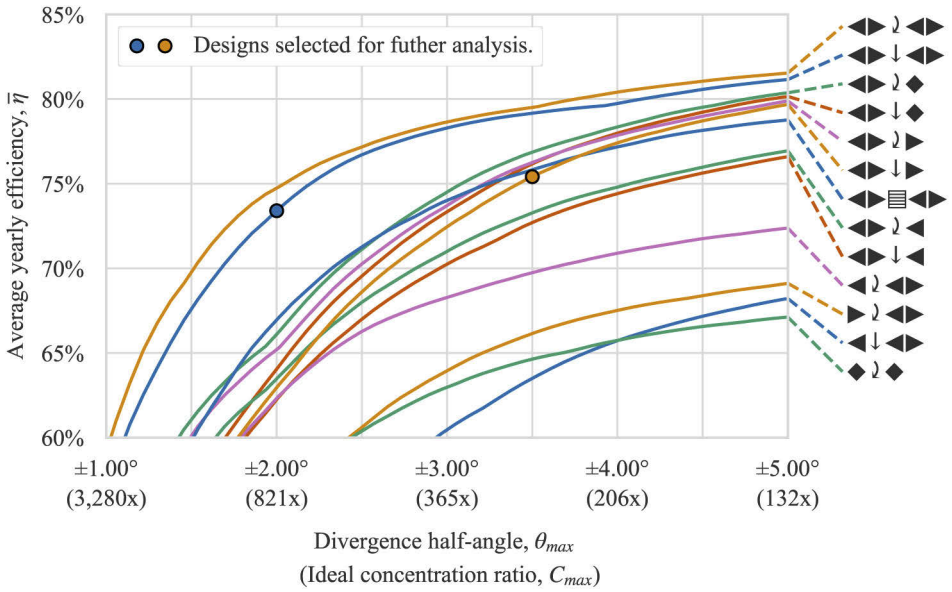

Fig. 5. Set of the best performing optimized configurations, mapping out the trade-off between efficiency and divergence half-angle. The value in brackets below the divergence half angle represents the ideal geometric concentration at this divergence half-angle, according to Eq. (3).

Due to the number of optimized configurations, only the best-performing configurations are shown in Fig. 5. The full set is available in Fig. 11.

Optics EXPRESS

4.1. Selected results

Each point along the lines in Fig. 5 represents a separate beam-steering lens array design. We report on two of those designs in more detail, representing different trade-offs between efficiency, divergence, and complexity. The first result is a ◄►↓◄► configuration optimized for a divergence half-angle of ±2°, which achieves 73.4% average yearly efficiency. This represents a configuration with high complexity, low divergence, and high efficiency. The result is highlighted with a blue circle in the Pareto fronts in Fig. 5, and a ray-traced drawing of the system can be seen in Fig. 6. Simulated efficiency across the tracking range is shown in Fig. 8(a) and is overlaid with a yearly irradiation distribution in Fig. 8(b).

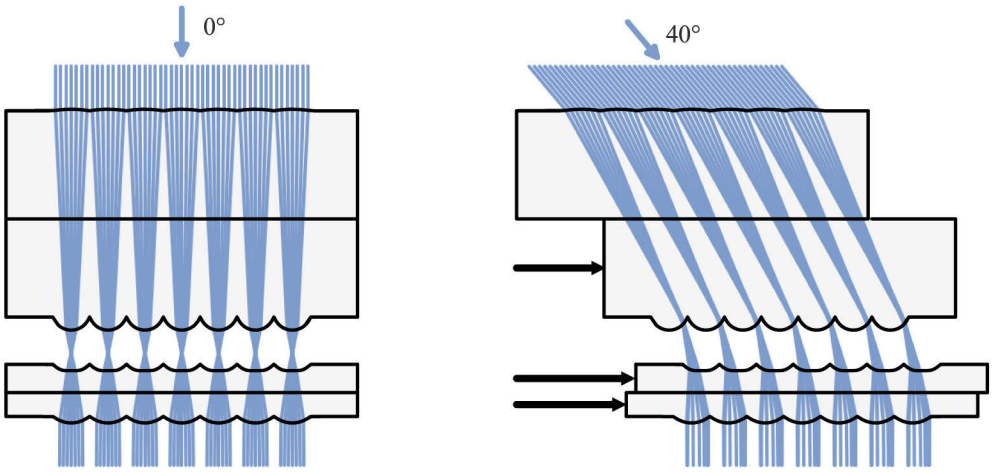

Fig. 6. Beam-steering lens array with ◄►↓◄► configuration optimized for 2° divergence half-angle (● in Fig. 5), drawn at 0° and 40° angles of incidence respectively. The black arrows indicate tracking motion. The drawing shows a 2 -dimensional slice of the optimized system, which consists of hexagonally packed three-dimensional lens arrays.

The second result is a ◄►↓► configuration optimized for ±3.5° divergence half-angle, which achieves 75.4% average yearly efficiency. This is an example of a system where a lower mechanical complexity is traded for a higher permitted divergence half-angle. The result is highlighted with a brown circle in the Pareto front in Fig. 5, and a ray-traced drawing of the system can be seen in Fig. 7. Simulated efficiency across the tracking range is shown in Fig. 8(a), and is overlaid with a yearly irradiation distribution in Fig. 8(b).

A ray-traced 3D model of the two selected designs is shown in Fig. 9. Zemax OpticStudio models are available as we show in Code 1 (Ref. [41]), and a comparison between the Zemax OpticStudio models and the internal ray-tracer models are included in Appendix C.

4.2. Influence of position and slope errors

To investigate the influence of position and slope errors on the optimization results, the ◄►↓◄► design was optimized for a set of error distributions with magnitudes different from the ones described in Table 3. The Pareto fronts for the different error distributions is shown in Fig. 10(a), while a tolerance analysis of selected designs is shown in Fig. 10(b). In addition, all configurations were also optimized for nominal performance assuming no errors, and the resulting Pareto fronts are included in Fig. 12 in Appendix B.

Optics EXPRESS

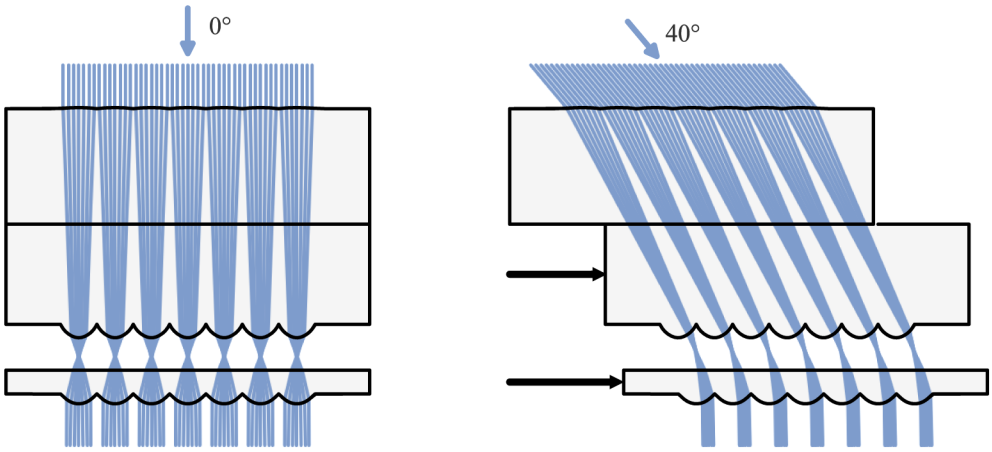

Fig. 7. Simplified beam-steering lens array with ◀▶↓▶ configuration optimized for 3.5° divergence half-angle (● in Fig. 5), drawn at 0° and 40° angles of incidence respectively. The black arrows indicate tracking motion. The drawing shows a 2-dimensional slice of the optimized system, which consists of hexagonally packed three-dimensional lens arrays.

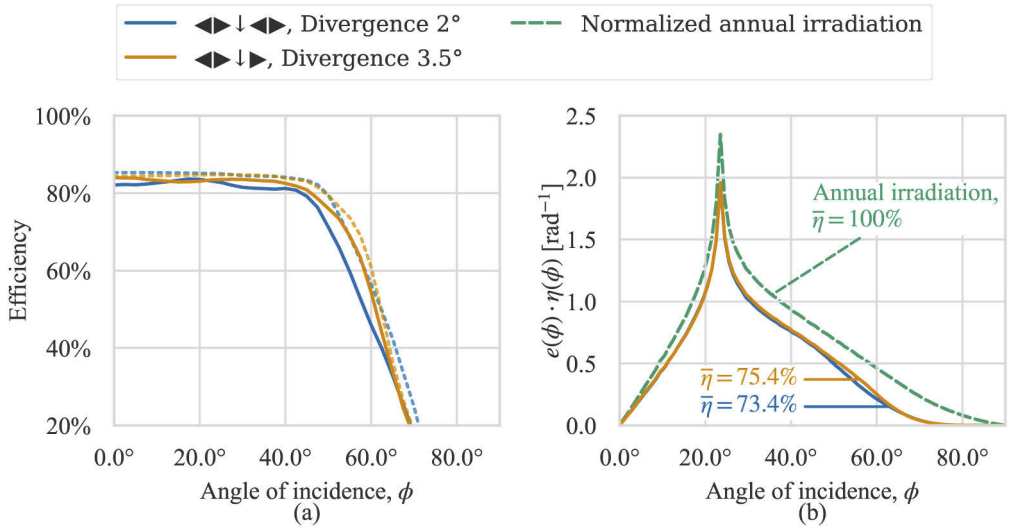

Fig. 8. (a) The two selected beam-steering lens arrays have >80% efficiency for ±40° angle of incidence, and a gradual drop-off in efficiency at larger angles of incidence. The dashed curves show nominal performance, while the continuous curves show expected performance with the chosen set of error distributions. (b) When the systems are placed in a fixed orientation as described in Section 3.2, this efficiency distribution corresponds to average yearly efficiency of 73.5% for the high concentration design and 75.6% for the simplified design, respectively.

Optics EXPRESS

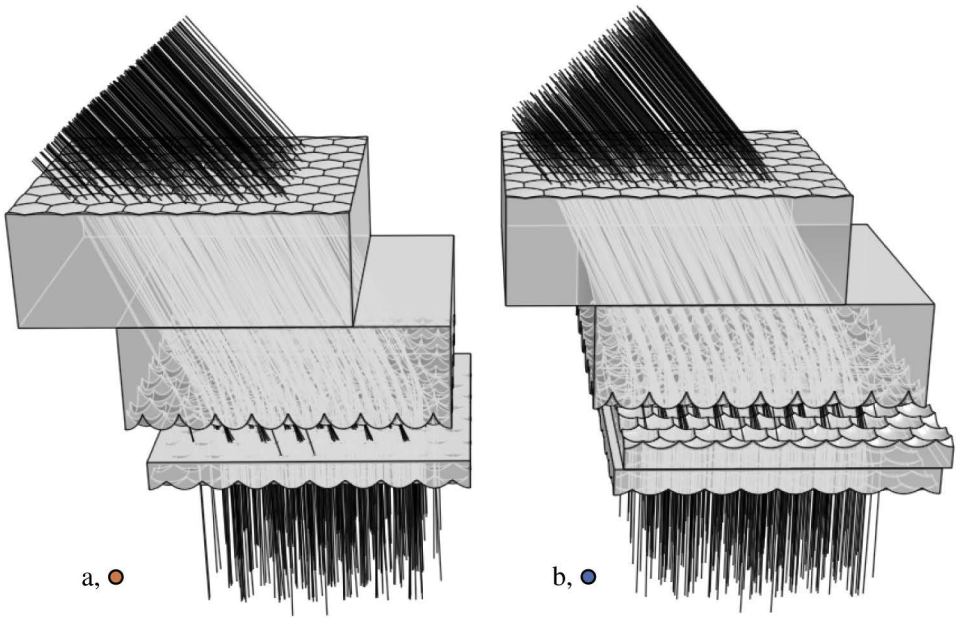

Fig. 9. Ray-traced 3D-model of the two selected beam-steering lens arrays, both shown at a 40° angle of incidence. (a) ◄►↓► configuration optimized for a permitted divergence of 3.5°, (b) ◄►↓◄► configuration optimized for a permitted divergence of 2.0°.

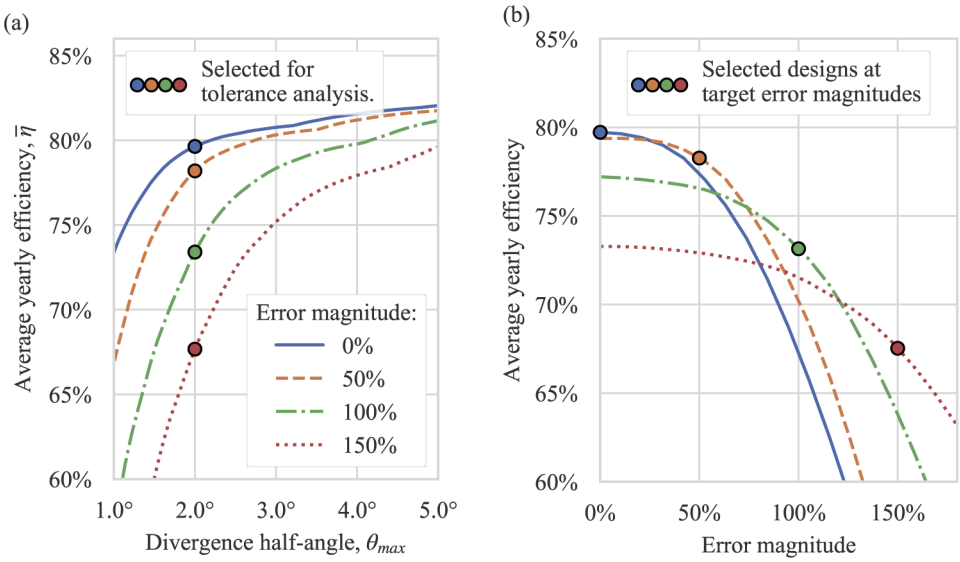

Fig. 10. (a) Optimized Pareto fronts for the ◄►↓◄► configuration, assuming different scaled versions of the error distributions in Table 3. 100% corresponds to the values reported in the table. The achievable performance is strongly influenced by the scale of manufacturing errors, as can be seen by the large changes to the Pareto fronts. (b) The selected designs from *a* are simulated at different error distributions to see how sensitive they are to errors. The system optimized for nominal performance has the highest performance at zero manufacturing errors, but is also the most sensitive to such errors.

Optics EXPRESS

5. Discussion

Stationary solar tracking requires beam-steering lens arrays with a wide dual-axis tracking range, making it difficult to rely on paraxial models and experience from conventional optical design to choose the ideal configuration. The use of numerical multi-objective optimization has enabled screening of many different configurations, to identify designs that are promising for future implementations of this concept.

The optimization results show that fairly complex optical systems are required to achieve high efficiency and low divergence for stationary solar tracking. The complex ◀▶⤸◀▶ and ◀▶↓◀▶ configurations outperform all the other configurations in Fig. 5 across the entire Pareto front.

At higher permitted divergence half-angles, some additional systems achieve relatively high efficiency, more specifically the class of systems starting with a ◀▶-pair of single-sided lens arrays.

Simpler configurations with only 1 moving surface, such as ◆⤸◆ or ◀▶ do not have the required degrees of freedom to enable high-efficiency stationary solar tracking. As seen in Fig. 5, the ◆⤸◆ configuration only achieves 67% average yearly efficiency when divergence half-angle is permitted to be as high as ±5.00°.

The selected results presented in Section 4.1 represent two different prioritizations of the different objectives, and they represent designs that we believe might be of interest for solar energy applications. The high-complexity ◀▶↓◀▶ design in Fig. 6 redirects sunlight into a narrow cone of ±2° divergence. It may therefore be relevant for high concentration applications, such as concentrator photovoltaics (CPV) or high-temperature concentrated solar power (CSP) applications. Figure 5 shows how even higher performance can be achieved with a ◀▶⤸◀▶ configuration, but the additional complexity in implementing a curved tracking trajectory might not be worth the relatively minor improvements to performance.

The selected ◀▶↓▶ design offers a simpler mechanical implementation with 3 lens arrays instead of 4. This reduced complexity comes at the cost of increased permitted divergence half-angle. The permitted divergence angle of ±3.5° represents a geometric concentration limit of 268x according to Eq. (3), which is still 26% higher than the $\frac{1}{sin(0.27°)} \approx 212$ concentration limit of conventional linear trough concentrators with single-axis tracking [2]. We therefore believe that this design might be of interest for low- to medium temperature CSP applications.

The beam-steering lens arrays demonstrated here emit collimated and redirected sunlight. To be used in CSP or CPV applications, these devices must be combined with a solar concentrator, for instance in the configuration illustrated in Fig. 1(a). An investigation into the best way to add such a concentrator, as well as a comparison of the resulting performance compared to other tracking-integrated solar concentrators, will be of interest for future development of this concept.

5.1. Optimizing for as-built performance

As described in Section 3.5, the systems were optimized for as-built performance by estimating the expected efficiency under the influence of manufacturing errors. Optimizing the systems for as-built performance is important because a system optimized for nominal performance can be very sensitive to manufacturing errors, while a system with slightly lower nominal performance may exhibit significantly lower sensitivity to surface errors [42]. We consider optimization for as-built performance to be especially important in the type of screening performed in this work, in order to not unrealistically favor highly complex configurations that may turn out to require very strict manufacturing tolerances. This effect is demonstrated in the tolerance analysis in Fig. 10(b): The system optimized for nominal performance is more sensitive to errors than systems optimized for as-built performance.

The optimization results are strongly affected by the chosen error distributions, as seen in Fig. 10(a), where the same configuration has been optimized for different error distributions. The distributions in this work were chosen as an example to demonstrate how the systems can

Optics EXPRESS

be optimized while taking manufacturing errors into account, and as a common ground for comparing the different beam-steering lens array configurations. When planning a real-world implementation of a beam-steering lens array, these error distributions should be updated to more accurately match selected manufacturing tolerances of the chosen lens molding process and system assembly.

Due to the strong influence of the error distributions, it can be difficult to compare the results in Fig. 5 with other related work optimized for different tolerances, or for nominal performance. For this reason, we have also included Pareto fronts optimized for nominal performance, available in Fig. 12 in Appendix B. The nominal results in Fig. 12 can be useful for comparing the beam-steering lens array configurations in this work against other alternatives optimized for nominal performance. However, we expect the nominal designs to be too sensitive to manufacturing errors to be used as a basis a physical beam-steering lens array, and therefore keep them outside the main body of the paper.

5.2. Implementation

There is no universally accepted way to optimize an optical system for reduced sensitivity to manufacturing errors, and different optical design software packages have implemented different heuristics to try to achieve this goal [42]. The task is especially challenging in conventional optical design, where the design of each individual system is of interest. In these designs, tolerance analysis is typically performed by sampling each surface error from the manufacturing tolerances, before applying an error compensation such as a refocus and simulating the resulting performance of the whole system. In the case of a beam-steering lens array, on the other hand, the object of interest is the combined average performance of the full set of lenses in the lens arrays, each subject to their own set of errors. We have therefore chosen to directly integrate the error distributions into the objective function by including them in the quasi-Monte Carlo integration of Eq. (7). In this way, each ray traced through the system is subject to a unique set of manufacturing errors sampled from the error distribution. This approach enables fast calculation of the average performance of a system subject to the selected error distributions, allowing the estimate to be directly used during optimization.

Unlike conventional tolerance analysis, our approach does not enable the use of compensators. The estimate might, therefore, be too pessimistic when estimating the influence of lateral positioning errors, which can likely be partially compensated for by the closed-loop tracking system in a physical realization of a beam-steering lens array. When planning a real-world implementation of a beam-steering lens array, the resulting design should therefore also be subjected to conventional tolerance analysis to more accurately validate the predicted as-built performance.

5.3. Multi-objective optimization

The use of a multi-objective optimization algorithm has enabled a comprehensive screening a large number of configurations of beam-steering lens arrays for stationary solar tracking, without having to make an upfront decision for the trade-off between permitted divergence angle and efficiency.

The permitted divergence angle is related to the achievable concentration ratio through Eq. (3). The trade-off curves in Fig. 5 are therefore a representation of the efficiency-versus-concentration curves known from Nonimaging Optics [2], and the objective function in Eq. (4) can be considered a special case of the overall problem in Nonimaging Optics of simultaneously optimizing both efficiency and concentration. The use of multi-objective optimization algorithms may, therefore, be of general interest to several problems in the field of Nonimaging Optics, and may constitute a topic of further future investigation beyond the topic of beam-steering lens array design.

Optics EXPRESS

6. Conclusions

We have performed a thorough screening of beam-steering lens array configurations in order to identify the most promising configurations for stationary solar tracking applications. This was enabled by using a set of symbols to specify and generate each configuration, and optimizing each configuration using multi-objective numerical optimization. The multi-objective optimization approach has enabled the optimization of beam-steering lens arrays without having to make an up-front decision for the trade-off between efficiency and divergence. The approach also enables the handling of manufacturing constraints and expected manufacturing errors, and may be of interest for other design problems in the field of nonimaging optics.

From this screening, we have identified beam-steering lens array designs capable of high efficiency full-day stationary solar tracking, and we specifically picked out two designs that might be candidates for solar energy applications. The first design has relatively high mechanical complexity with 4 optical surfaces, and can be suitable for high-concentration applications, achieving 73.4% average yearly efficiency in redirecting sunlight into a $<2^\circ$ divergence half-angle. The second system has lower complexity, with 3 optical surfaces, and may be suitable for low-concentration applications. It achieves 75.4% average yearly efficiency in redirecting sunlight into a $<3.5^\circ$ divergence half-angle. These reported configurations may contribute to the development of low-cost tracking-integrated solar energy, and further the development of tracking-integrated solar concentrators.

Optics EXPRESS

Appendix A Full optimization results

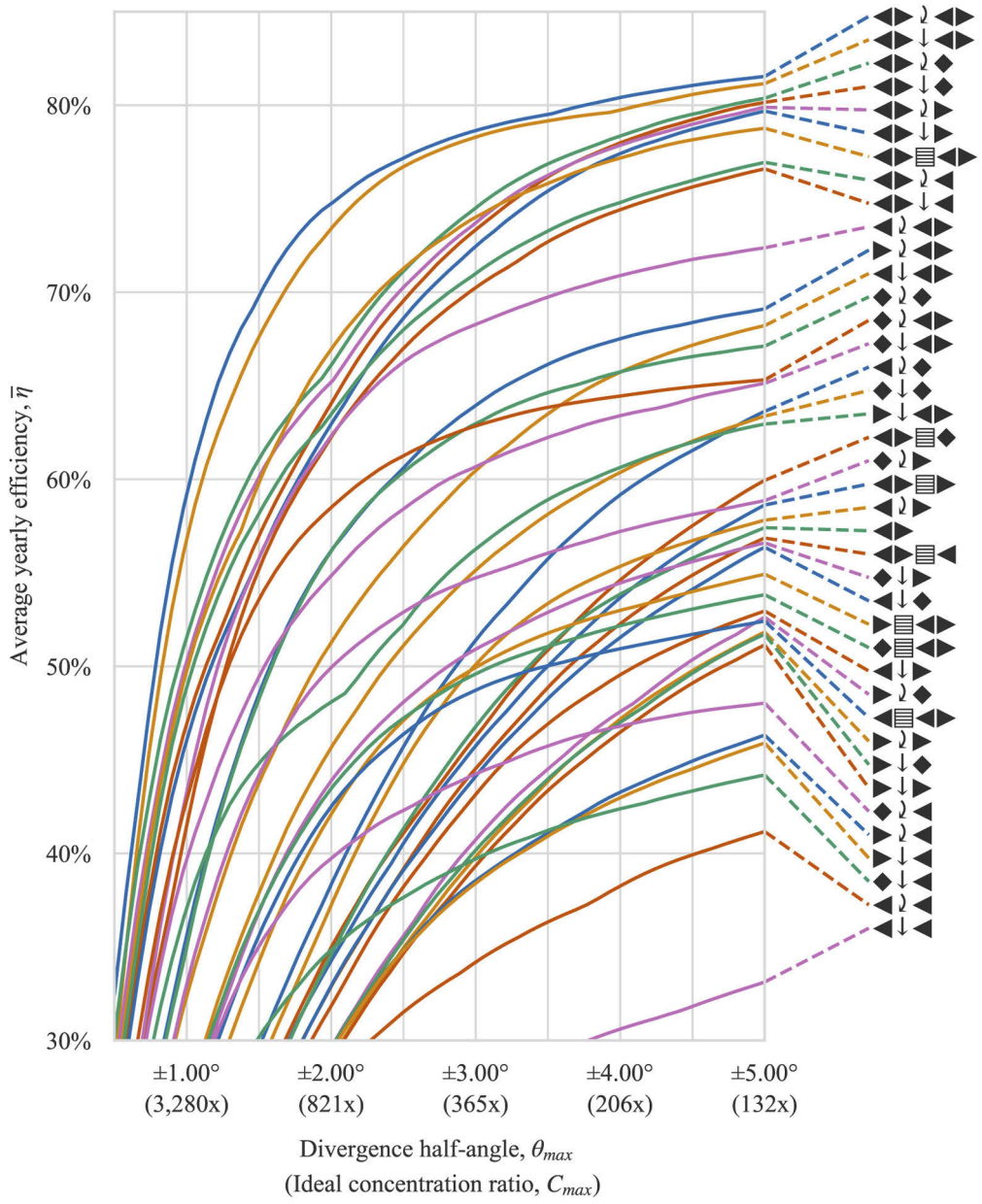

Fig. 11. Full set of trade-off curves for different configurations of beam-steering lens arrays optimized as described in Section 3.5.

Optics EXPRESS

Appendix B Full optimization results optimized for nominal performance

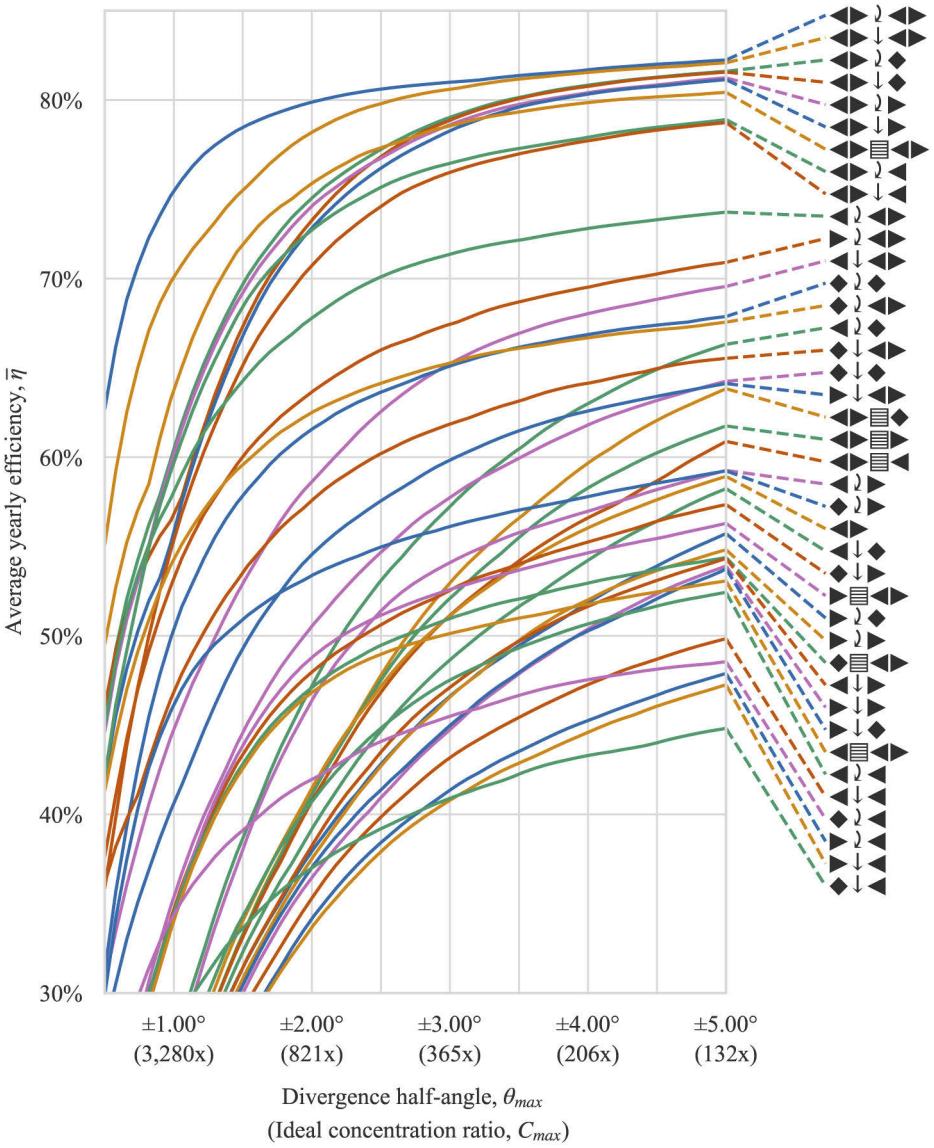

Fig. 12. Full set of trade-off curves for different configurations of beam-steering lens arrays optimized as described in Section 3.5, but assuming nominal performance instead of as-built performance.

Appendix C Details on Zemax OpticStudio model

Zemax OpticStudio models of the two selected beam-steering lens array designs is available in the supplementary materials Code 1 (Ref. [41]). These models are used to document and verify the designs, and also used to create the 3D models in Fig. 9. However, due to limitations in Zemax OpticStudio, the models do not capture the full complexity of the Python ray-tracer used during optimization.

Optics EXPRESS

The Zemax OpticStudio model includes a Merit Function used to evaluate optical efficiency at the discrete set of angle of incidence. This merit function is used to verify the performance of the beam-steering lens arrays, as shown in Fig. 13. However, the merit function does not implement the design method described in Section 3, and is not suitable for optimization using the built-in optimization algorithms in Zemax OpticStudio, which do not support multi-objective optimization.

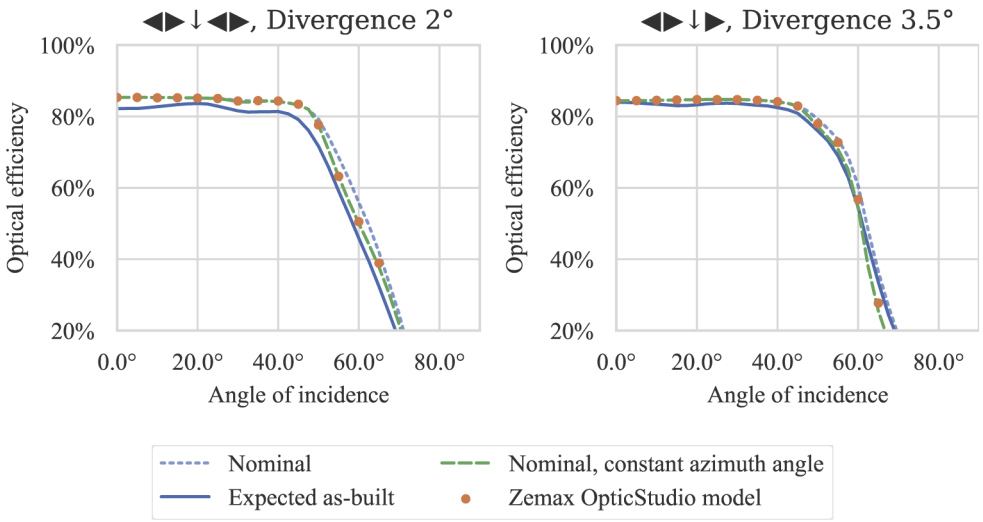

Fig. 13. Comparing internal Python model and Zemax OpticStdio model of the selected beam-steering lens array designs. The Zemax OpticStudio model assumes nominal performance and constant azimuth angle, and the simulated efficiencies agree well with the internal Python model when these assumptions are replicated.

The efficiency estimate from Zemax OpticStudio contains the following set of simplifications compared to the Python model:

- Tracking motion is represented at a set of discrete angles of incidence using the multi-configuration functionality in Zemax OpticStudio. During optimization, tracking motion is represented as a continuous function of angle of incidence.
- The builtin PMMA material model in Zemax OpticStudio is only defined between 365nm and 1060nm, and the AM1.5D solar spectrum is therefore clipped to this range. During optimization, the whole AM1.5D spectrum is used.
- For simplicity, the Zemax OpticStudio model only demonstrates solar tracking across 1 axis – in other words, with a constant azimuth angle. Since lenslets are packed hexagonally and thus not completely rotationally symmetric, tracking performance is not fully uniform across different azimuth angles. During optimization, the azimuth angle is included as an integration dimension in the multi-dimensional quasi-Monte Carlo integration of Eq. (7).
- The Zemax OpticStudio model estimates nominal system performance, not as-built performance, as discussed in Section 5.1.
- During optimization, the lenslet surfaces are represented using 8th order Forbes' Q^{con} surfaces [40]. When creating the Zemax OpticStudio models, this representation is converted to an even polynomial representation, in order to be represented as Zemax OpticStudio's "Hexagonal Lenslet Array" object type.

Optics EXPRESS

- The Zemax OpticStudio system is modeled as a lens array with 9 by 9 lenslets, and the source is modeled as a rectangular source aimed towards this array. There might therefore be small edge-effects, where some of the lenslets are only partially illuminated. During optimization, an infinite array of lenslets is assumed.

Acknowledgments

Portions of this work were presented at the *SPIE Optical Engineering + Applications* conference in 2019, paper number 111200B [15], and at the *SPIE Optical Engineering + Applications* conference in 2018, paper number 1075805 [14].

Disclosures

The authors declare no conflicts of interest.

References

1. W. T. Xie, Y. J. Dai, R. Z. Wang, and K. Sumathy, "Concentrated solar energy applications using Fresnel lenses: A review," Renewable Sustainable Energy Rev. **15**(6), 2588–2606 (2011).
2. R. Winston, J. C. Minano, P. G. Benitez, W. N. Shatz John, C. Bortz, and J. C. Bortz, *Nonimaging Optics* (Elsevier Science, 2005).
3. H. Apostoleris, M. Stefancich, and M. Chiesa, "Tracking-integrated systems for concentrating photovoltaics," Nat. Energy **1**(4), 16018 (2016).
4. F. Duerr, Y. Meuret, and H. Thienpont, "Tracking integration in concentrating photovoltaics using laterally moving optics," Opt. Express **19**(S3), A207–A218 (2011).
5. F. Duerr, Y. Meuret, and H. Thienpont, "Tailored free-form optics with movement to integrate tracking in concentrating photovoltaics," Opt. Express **21**(S3), A401–A411 (2013).
6. A. J. Grede, J. S. Price, and N. C. Giebink, "Fundamental and practical limits of planar tracking solar concentrators," Opt. Express **24**(26), A1635–A1646 (2016).
7. P. Kotsidas, V. Modi, and J. M. Gordon, "Nominally stationary high-concentration solar optics by gradient-index lenses," Opt. Express **19**(3), 2325–2334 (2011).
8. V. Narasimhan, D. Jiang, and S.-Y. Park, "Design and optical analyses of an arrayed microfluidic tunable prism panel for enhancing solar energy collection," Appl. Energy **162**, 450–459 (2016).
9. L. D. DiDomenico, "Towards doubling solar harvests using wide-angle, broad-band microfluidic beam steering arrays," Opt. Express **23**(24), A1398–A1417 (2015).
10. N. León, C. Ramírez, and H. García, "Rotating Prism Array for Solar Tracking," Energy Procedia **57**, 265–274 (2014).
11. S. Valyukh, I. Valyukh, and V. Chigrinov, "Liquid-Crystal Based Light Steering Optical Elements," Photonics Lett. Pol. **3**(2), 88–90 (2011).
12. R. Campbell and M. Machado, "LOW cost CPV = Embedded CPV with internal tracker," in *2010 35th IEEE Photovoltaic Specialists Conference*, (IEEE, 2010), pp. 003003–003007.
13. W. Lin, P. Benitez, and J. C. Miñano, "Beam-steering array optics designs with the SMS method," Proc. SPIE **8485**, 848505 (2012).
14. H. J. D. Johnsen, J. Torgersen, and A. Aksnes, "Solar tracking using beam-steering lens arrays," Proc. SPIE **10758**, 4 (2018).
15. H. J. D. Johnsen, A. Aksnes, and J. Torgersen, "Pushing the limits of beam-steering lens arrays," Proc. SPIE **11120**, 10 (2019).
16. K. M. Flood, B. Cassarly, C. Sigg, and J. Finlan, "Continuous wide angle beam steering using translation of binary microlens arrays and a liquid crystal phased array," Proc. SPIE **1211**, 296–304 (1990).
17. E. A. Watson, "Analysis of beam steering with decentered microlens arrays," Proc. SPIE **32**(11), 2665–2670 (1993).
18. A. Akatay, C. Ataman, and H. Urey, "High-resolution beam steering using microlens arrays," Opt. Lett. **31**(19), 2861–2863 (2006).
19. S. A. Kalogirou, *Solar Energy Engineering: Processes and Systems* (Academic, 2013).
20. J. Bourderionnet, M. Rungenhagen, D. Dolfi, and H. D. Tholl, "Continuous laser beam steering with micro-optical arrays: Experimental results," Proc. SPIE **7113**, 71130Z (2008).
21. J. Xiang, N. Wu, J. Zhang, and L. Wu, "Design of driving and control system based on Voice Coil Actuation for linear motion of micro-lens array," Proc. SPIE **7133**, 713330 (2009).
22. I. Ono, S. Kobayashi, and K. Yoshida, "Global and multi-objective optimization for lens design by real-coded genetic algorithms," Proc. SPIE **3482**, 110–121 (1998).
23. Bráulio Fonseca Carneiro de Albuquerque, F. L. de Sousa and A. S. Montes, "Fonseca Carneiro de Albuquerque Multi-objective approach for the automatic design of optical systems," Opt. Express **24**(6), 6619–6643 (2016).

Optics EXPRESS

24. C. C. Olson, "Automated design of optical architectures using novel encoding methods and a multi-objective optimization framework," Proc. SPIE **11105**, 11 (2019).
25. P. M. Pardalos, A. Žilinskas, and J. Žilinskas, *Non-Convex Multi-Objective Optimization, Springer Optimization and Its Applications* (Springer International Publishing, 2017).
26. A. Ito, D. Sato, and N. Yamada, "Optical design and demonstration of microtracking CPV module with bi-convex aspheric lens array," Opt. Express **26**(18), A879–A891 (2018).
27. C. S. Schuster, "The quest for the optimum angular-tilt of terrestrial solar panels or their angle-resolved annual insolation," Renewable Energy **152**, 1186–1191 (2020).
28. A. B. Meinel and M. P. Meinel, *Applied Solar Energy: An Introduction* (Addison-Wesley, 1976).
29. J. S. Price, X. Sheng, B. M. Meulblok, J. A. Rogers, and N. C. Giebink, "Wide-angle planar microtracking for quasi-static microcell concentrating photovoltaics," Nat. Commun. **6**(1), 6223 (2015).
30. E. Watson, D. Miller, and K. Barnard, "Analysis of fill factor improvement using microlens arrays," Proc. SPIE **3276**, 123–134 (1998).
31. J. Duparré, D. Radtke, and P. Dannberg, "Implementation of field lens arrays in beam-deflecting microlens array telescopes," Appl. Opt. **43**(25), 4854–4861 (2004).
32. Unicode Consortium, The Unicode Standard, Version 12.0 (2019).
33. H. Li and Q. Zhang, "Multiobjective Optimization Problems With Complicated Pareto Sets, MOEA/D and NSGA-II," IEEE Trans. Evol. Computat. **13**(2), 284–302 (2009).
34. J. Blank and K. Deb, "Pymoo: Multi-Objective Optimization in Python," IEEE Access **8**, 89497–89509 (2020).
35. P. Virtanen, R. Gommers, T. E. Oliphant, M. Haberland, T. Reddy, D. Cournapeau, E. Burovski, P. Peterson, W. Weckesser, J. Bright, S. J. van der Walt, M. Brett, J. Wilson, K. J. Millman, N. Mayorov, A. R. J. Nelson, E. Jones, R. Kern, E. Larson, C. J. Carey, İ. Polat, Y. Feng, E. W. Moore, J. VanderPlas, D. Laxalde, J. Perktold, R. Cimrman, I. Henriksen, E. A. Quintero, C. R. Harris, A. M. Archibald, A. H. Ribeiro, F. Pedregosa, P. van Mulbregt, and S. . Contributors, "SciPy 1.0: Fundamental algorithms for scientific computing in Python," Nat. Methods **17**(3), 261–272 (2020).
36. D. Kraft, "A software package for sequential quadratic programming," Tech. Rep. DFVLR-FB 88-28, DLR German Aerospace Center – Institute for Flight Mechanics (Koln Germany, 1988).
37. J. Köster and S. Rahmann, "Snakemake—a scalable bioinformatics workflow engine," Bioinformatics **28**(19), 2520–2522 (2012).
38. Renewable Resource Data Center, Solar Spectral Irradiance: Air Mass 1.5, https://rredc.nrel.gov/solar/spectra/am1.5/.
39. D. Buie, A. G. Monger, and C. J. Dey, "Sunshape distributions for terrestrial solar simulations," Sol. Energy **74**(2), 113–122 (2003).
40. G. W. Forbes, "Shape specification for axially symmetric optical surfaces," Opt. Express **15**(8), 5218–5226 (2007).
41. H. J. D. Johnsen, A. Aksnes, and J. Torgersen, "Zemax OpticStudio Models of Beam-Steering Lens Arrays, figshare," (2020). https://doi.org/10.6084/m9.figshare.12505784
42. K. E. Moore, "Optimization for as-built performance," Proc. SPIE **10925**, 1 (2019).